

AIAA-2000-2450

**PIV Investigation of Role of Boundary
Layer Velocity Fluctuations in Unsteady
Shock-Induced Separation**

Ö. H. Ünalmiş, Y. X. Hou, P. C. Bueno
N. T. Clemens, and D. S. Dolling
Center for Aeromechanics Research
The University of Texas at Austin
Austin, Texas 78712-1085

21st AIAA Aerodynamic Measurement
Technology and Ground Testing Conference
June 19-22, 2000 / Denver, CO

PIV Investigation of Role of Boundary Layer Velocity Fluctuations in Unsteady Shock-Induced Separation

Ö. H. Ünalmsis,^{*} Y. X. Hou,⁺ P. C. Bueno,⁺ N. T. Clemens,[†] and D. S. Dolling,[‡]

Center for Aeromechanics Research

Department of Aerospace Engineering & Engineering Mechanics

The University of Texas at Austin

Austin, Texas 78712-1085

Abstract

Particle image velocimetry measurements have been made in conjunction with fluctuating wall pressure measurements in a blunt fin-induced interaction in a Mach 5 flow. Results show that the separation shock foot motion correlates with the velocity fluctuations in the lower part of the boundary layer: positive fluctuations are associated with downstream motions of the shock foot, whereas negative fluctuations are associated with upstream motions of the shock foot. These results are consistent with an earlier study in the same facility with a compression ramp model.

Introduction

Experiments from a wide range of test facilities, from continuous to intermittent, from transonic to hypersonic, have shown that shock-induced turbulent boundary layer separation is a highly unsteady process, especially in large-scale 2-D or axisymmetric flows. The unsteadiness is important from both an applications and a modeling perspective. Maximum fluctuating pressure levels and thermal loads that a structure is exposed to are generally found in regions of shock/boundary layer and shock/shear layer interaction and can affect vehicle and component geometry, structural integrity, material selection, fatigue life, the design of thermal protection systems, weight, and cost. From a modeling perspective Knight and Degrez¹ have identified "unsteadiness" as one of the key reasons for the poor comparisons of simulation and experiment for strong interactions. Over the past 15-20 years there have

been a significant number of studies focussing on documenting the details of the unsteadiness for a range of model configurations, and on investigating the underlying causes of the unsteadiness. Much of the work up until the early 1990's is reviewed in Ref. 2. Currently it is fair to say that the experimental data still cannot be fitted into, and understood, within a comprehensive framework. A very brief summary of some of this earlier work, together with more recent findings is given below.

Experimental work³⁻⁷ in an unswept compression ramp interaction has shown that the separation shock foot motion and hence the expansion/contraction (or pulsation) of the separated flow has two primary components: low frequency, large-scale motion and high frequency, small-scale motion. Fig. 1 shows an example of the separation shock foot history in a piecewise continuous form for a 28° unswept compression ramp flow at Mach 5. This was deduced from the analysis of eight simultaneously sampled wall pressure signals. The analysis technique^{5,8} is based on a box-car representation of the intermittent surface pressure signals. With a small spacing between transducers the shock foot position can be bracketed reasonably accurately. As can be seen from Fig. 1b, the low and high frequency motions of the separation shock are superposed on each other and there is no clear demarcation between them.

Erengil and Dolling⁶ examined separation shock foot unsteadiness in different 2-D and 3-D interactions and concluded that the separation shock unsteadiness can be attributed to two different physical phenomena: 1) The small-scale motion of the separation shock is caused by its response to fluctuations in the ratio of static quantities across the shock foot induced by passage through the shock of "turbulent structures" in the incoming boundary layer, and 2) The large-scale motion of the separation shock is caused by its displacement due to the expansion and contraction motion of the separated flow. However, part 2) above is simply an observation and does not explain why the separation bubble undergoes this low frequency, large-scale expansion/contraction motion. A reasonable question is whether some low frequency *component* in the boundary layer induces the

^{*} Research Associate, Member AIAA

⁺ Graduate Student, Student Member AIAA

[†] Associate Professor, Senior Member AIAA

[‡] Professor, Fellow AIAA

Copyright © 2000 by Ö.H. Ünalmsis, Y.X. Hou,

P.C. Bueno, N.T. Clemens, and D.S. Dolling.

Published by the American Institute of Aeronautics and Astronautics, Inc. with permission.

expansion/contraction motion. Some evidence in support of that idea comes from the work of McClure.⁷ He used the same unswept compression ramp model under the same flow conditions as was used in Ref. 6. In one of his experiments the signal from a small, high frequency response Pitot probe mounted far upstream ($\approx 16 d_0$) of the compression corner was recorded simultaneously with wall pressure signals under the separation shock. Ensemble-averaged Pitot pressure histories were then calculated for upstream and downstream sweeps of the separation shock. For Pitot probe heights less than about $0.9 d_0$, there was a gradual decrease in Pitot pressure (about 5%) during an upstream shock motion and a gradual increase (about 5%) during a downstream shock motion. The time-scale of the shock motions and the corresponding rises and falls in Pitot pressure were of the order of 1ms. It is interesting to note that during such a time interval the freestream flow travels almost 1m and, assuming large-scale turbulent structures have a streamwise length scale of order d_0 , 20–40 such structures pass by a fixed point in the interaction. Based on the long duration variation in Pitot pressure with certain shock foot motions it was hypothesized that the boundary layer has a low frequency behavior which is connected to the shock and the separated flow expansion/contraction.

Re-analysis of McClure's data by Ünalmiş and Dolling⁹ (Fig. 2) shows that when the separated flow is at its maximum size, the average Pitot pressure in the upstream boundary layer at a fixed height above the wall is lower than the mean Pitot pressure at that point and the opposite is true when the separated flow is at its minimum size. Low intermittency in the figure (where intermittency is defined as the percentage of time that the separation shock foot is upstream of a given point) corresponds to the shock foot far forward. The fact that the ensemble-averaged Pitot pressure has different values for the two extreme scales of the separated flow initially suggested a very simple model involving a low frequency "thickening/thinning" motion of the boundary layer. When the boundary layer thickens, the fixed Pitot probe would read a lower value since its effective height in the boundary layer decreases. The opposite would be true for a thinning motion of the boundary layer. However, more recent work using planar laser scattering and particle image velocimetry in the same flowfield, discussed further below, suggests that this simple model is incorrect.¹⁰⁻¹¹

Work by Marshall and Dolling¹² in compression ramp interactions has shown that the spanwise rippling of the shock foot remained coherent over a distance of order $2 d_0$ which is not consistent with measured spanwise scales of turbulent structures in supersonic turbulent boundary layers.¹³ Based on these observations some

interesting questions were raised:¹⁴⁻¹⁶ If the shock foot motion were driven directly by the incoming flow itself, then what in the incoming boundary layer had a spanwise scale of order $2 d_0$? Alternatively, could an instability (perhaps triggered by the incoming flow) in the separated flow control the spanwise scale of the shock foot dynamics?

Analysis of cross-correlations of wall pressure signals by Ünalmiş¹⁴ and Ünalmiş and Dolling¹⁵⁻¹⁶ have since shown the existence of a spanwise vortex structure in the incoming boundary layer. The spanwise scale of the periodicity of this vortex structure was about $2 d_0$. To explore these findings further, Ünalmiş and Dolling¹⁵⁻¹⁶ conducted a series of experiments in which a triple-tipped Pitot probe (the tips were separated spanwise) was placed in the boundary layer far upstream of a blunt fin model (Fig. 3). They showed that the magnitude of the Pitot pressure in the incoming boundary layer correlates with the scale of the separated flow and that the trends seen in the ensemble-average Pitot pressure histories are independent of the direction of the shock foot motion but closely correlated with the extreme positions of the shock foot. Furthermore, they observed that the various tips of the probe had different trends. For example, while the center probe had an increasing pressure on the order of 1 ms the side probes had the opposite trends (Fig. 4). Cross correlation of the signals from the tips confirmed this finding; yielding a negative correlation between the side probes and the center probe. Based on their findings Ünalmiş and Dolling suggested that the spanwise vortex structure in the incoming boundary layer, such as Görtler vortices caused by the concave curvature of the nozzle, might be at least one of the causes of the low frequency pulsation of the separated flow.

Recently, Beresh *et al.*¹⁷⁻¹⁸ employed planar laser diagnostic techniques in combination with fast response pressure measurements in a compression ramp interaction, to further examine the role of the upstream boundary layer on the separation shock motion. Planar laser scattering (PLS) from a seeded alcohol fog was used to visualize turbulent structures interacting with the separation shock.¹⁷ The seeding density was sufficiently high that the shock foot could be seen in most of the images. Double-pulse image pairs, separated in time by 15 to 30 μ s, showed that large-scale structures in the upstream boundary layer would greatly distort the outer region of the separation shock, but the shock *foot* did not move appreciably in this time scale. This result is consistent with previous studies using wall pressure measurements, which report shock frequencies that do not exceed 10 kHz. They conclude from this that large-scale structures in the outer part of the boundary layer are not primarily

responsible for the motion of the separation shock. (This observation seems to differ from the observations of Wu and Miles¹⁹ who obtained 500 kHz image sequences (30 images) of a Mach 2.5 compression ramp interaction using planar Rayleigh scattering. They conclude that certain rare types of turbulent structures can cause the shock foot to move about a boundary layer thickness in extent).

In a following study, Beresh *et al.*¹⁸ applied the Particle Image Velocimetry (PIV) technique to investigate the role of upstream boundary layer velocity fluctuations on the separation shock motion in a Mach 5 compression ramp interaction. They acquired PIV images in the upstream boundary layer, while simultaneously monitoring the shock-foot position using wall pressure transducers. The PIV images were conditionally averaged based on several types of shock motions: no motion, upstream motion of 1,2, or 3 bins (where a bin is the distance between transducers), and downstream motion of 1, 2, or 3 bins. In order to investigate only particular bandwidth fluctuations, the shock motions were constrained to occur within a given time window (after accounting for the convection time from the PIV measurement location to the interaction). Time windows of 100, 250 and 500 μ s were used, corresponding to frequencies of 10, 4 and 2 kHz, respectively. The conditionally acquired PIV images were then used to generate transverse profiles of the mean velocity fluctuations for the different shock motions. An example result, for a 250 μ s time window (4 kHz), is shown in Fig. 5. The measurements show that away from the wall, the fluctuations average to zero, as is expected for a random event. It can be concluded from this result that the boundary layer is not undergoing a low-frequency thickening and thinning, as was suggested by Ünalms and Dolling⁹ (discussed above). However, nearer to the wall, the profiles diverge, showing that the positive streamwise velocity fluctuations in the upstream boundary layer are correlated with downstream shock foot motions and negative velocity fluctuations are correlated with upstream shock foot motions. Beresh *et al.*¹⁸ conclude that these results are consistent with the simple concept of a fuller velocity profile providing increased resistance to separation and thus a downstream shock foot position.

Overall, these results present a somewhat confusing picture. Although the proposed cause of the high-frequency, small-scale motion of the shock foot seems physically reasonable, the cause of the large-scale, low-frequency unsteadiness, which is of primary concern in modeling and engineering applications, is not yet clear. The boundary layer clearly has a low-frequency component and a 3-D structure, although the origin of this component and the importance of the three-dimensionality

is yet to be understood. An interesting question is whether this low-frequency component is a naturally occurring feature of a supersonic turbulent boundary layer or is a wind tunnel phenomenon which could be tunnel-specific. It should be noted that it is not unique to the Mach 5 blowdown tunnel used in the current experiment since the unsteadiness described above is seen in a wide variety of continuous and blowdown tunnels. This is an important question because the existing experimental data sets which are used to validate computations consist of mean surface and flowfield data which are time-averages of the unsteady properties. Should the character of the unsteadiness be a function of the facility, the time-averaged properties of a given interaction may also be facility-dependent.

Current Work

A recent study in a compression ramp-induced interaction has shown that significant correlations exist between the velocity fluctuations in the lower part of the incoming boundary layer and specific separation shock motions. It is well known that there are fundamental differences in the scaling of unsteady turbulent boundary layer separation induced by compression ramps and blunt fins. In the former the region of separation shock motion scales on d_0 whereas in the latter case it scales on the fin diameter D . Whereas in compression ramp flows this region is limited to about a boundary layer thickness in length, in the fin-induced interaction it can be tens of boundary layer thicknesses long. The blunt fin flowfield is characterized by an unsteady shock foot that wraps around the fin leading edge. Beneath this foot, the boundary layer separates and a complex horseshoe vortex system develops. This vortex system wraps about the fin root and trails downstream.²⁰⁻²²

Normalized cross-correlations of shock velocity and upstream wall pressure fluctuations in both blunt fin and compression ramp interactions have also shown some differences in the dynamics of these flowfields.^{6,23} Fig. 6 shows four different plots from four different geometries: two compression ramps (unswept and 25 deg sweep angle) and two blunt fins (8 and 30 deg sweep angles). In all cases there is a positive correlation at negative time delay. However, the blunt fin correlations also have smaller secondary peaks at earlier time-delays. This is because of the strong recirculation present in blunt fin interactions: turbulent structures pass through the separation shock and the separated shear layer, arrive at the fin root region, and are recirculated upstream, influencing the shock motion. Because not all the structures are recirculated upstream, and not all the recirculated ones remain coherent over such a distance,

the magnitude of the secondary peaks are smaller. All of these raise the question of whether the same mechanism seen in the ramp flows would also occur in the blunt fin flow, or would the possible presence of another more dominant mechanism, perhaps associated with fluctuations in the separated flow (which also scales on D) render correlations much weaker.

Experimental Program

Wind Tunnel and Flow Conditions

All of the experiments were conducted in the Mach 5 blowdown tunnel of the University of Texas at Austin. The constant-area test section is 6 in (15.2 cm) wide by 7 in (17.8 cm) high and has a length of 30 in (76.2 cm). Removable side doors allow access to the instrumented floor section. A total of about 140 ft³ (4 m³) of compressed air is provided by a Worthington HB4 four-stage compressor and stored in external tanks at a pressure of about 2500 psia (17.24 MPa). Two banks of nichrome wire resistive heaters (420 kW each) located upstream of the stagnation chamber heat the incoming air to the desired stagnation temperature, which is measured by a Type J thermocouple. These heaters can provide stagnation temperatures of up to 759 °R (422 K). The stagnation chamber pressure and temperature for the present experiments are approximately 325 psia (2.24 MPa ±1%) and 636 °R (353 K ±1%), respectively. For these stagnation conditions, stable run times of up to 1 minute can be obtained. The nominal properties of the incoming freestream flow in the test section are given in Table 1.

Table 1 Incoming Flow Conditions

M_∞	4.95	4.95
U_∞	2509 ft/s	765 m/s
Re_∞	$15.24 \times 10^6/\text{ft}$	$50 \times 10^6/\text{m}$
P_0	325 psia	2.24 MPa
T_0	636 °R	353 K

The incoming turbulent boundary layer undergoes natural transition and develops under approximately adiabatic wall temperature conditions. The *undisturbed* boundary layer thickness, d_0 , is based on the height in the boundary layer where the local velocity reaches 99% of the freestream value. The value of d_0 is 0.76 in. (1.93 cm).

Instrumentation and Data Acquisition

Fluctuating pressure measurements were made using Kulite Semiconductor Products, Inc., Model XCQ-062-50A and XCQ-062-15A transducers. These transducers have a nominal outer diameter of 0.0625 in (0.159 cm) and a pressure-sensitive diaphragm of 0.028 in (0.071 cm) in diameter. Perforated screens above the diaphragm protect the transducer from being damaged by dust particles in the flow but limit the frequency response of both models to about 50 kHz. For comparison, the characteristic frequency of the larger boundary-layer structures is expected to be of order U_∞/d_0 , which corresponds to a frequency of 40 kHz. The transducers were flush-mounted on a rectangular instrumentation plug, which also has an anti-reflection coated window about 2 in. (5.1 cm) upstream of the ports. Output from the Kulite pressure transducers was amplified by Dynamics (Model 7525) amplifiers. The amplified signals were then filtered using Ithaco (Models 4113 or 4213) analog filters. A sampling rate of 100 kHz was used in most of the experiments while the filter cut-off was set at 40 kHz. The signal-to-noise ratio was about 200.

Pressure data were acquired using two LeCroy analog-to-digital (A/D) converters with 12-bit resolution (Model 6810 waveform recorders). Each A/D converter has 4 megabytes of memory and can sample 1 channel of data at rates up to 5 MHz, or 4 channels of data simultaneously at rates up to 1 MHz per channel. The two A/D's can acquire data from 8 channels simultaneously when triggered using the same clock. For the current work 6 channels were used: The first 5 channels recorded the fluctuating pressure signals whereas the last one recorded the laser Q-switch signal for the first pulse. For the fluctuating pressure measurements only, 262144 data points were acquired per channel with a sampling frequency of either 50 or 100 kHz. For simultaneous fluctuating pressure and PIV measurements 4096 data points per channel were acquired for each PIV image. For simultaneous measurements the A/D converters were pre-triggered: once the laser fired, it triggered the A/D, and the A/D assigned the triggering time as the center of the total 4096 data points for each channel, and acquired 2048 data points before and after the triggering time. This way it was possible to avoid some synchronization problems due to the electronics and accurately match the timing of the image and pressure signals.

Blunt Fin Model

A hemicylindrically blunted fin of 0.75 in. (1.91 cm) leading edge diameter was used to generate the separated flow (Fig. 7). The fin is 4 in. (10.16 cm \approx 5.3 d_0) high and

has a 1.0 in. (2.54 cm) wide base extension which fits into a slot in the floor with screws underneath securing it in place. With the aid of 0.0576 in. (0.146 cm) long gauge blocks the distance between the fin leading edge and intermittent region transducers could be set accurately.

Fluctuating Pressure Measurements

The fluctuating pressure transducers and the model are placed on the floor centerline (Fig. 7). The transducers were placed in the intermittent region at 0.115 in. (0.29 cm) intervals such that the most downstream and the most upstream transducers were 1.83 in. (4.64 cm) and 2.29 in. (5.8 cm) upstream of the blunt fin leading edge, respectively.

In the analysis of the pressure data the two-threshold method⁸ was used to detect the shock events: when the pressure exceeds the upper threshold, the pressure rise is assumed to be due to the upstream passage of the separation shock foot over a given transducer. When the pressure falls below the lower threshold, the shock is assumed to move downstream of the transducer. The upper and the lower thresholds were chosen as $T_{hi} = \bar{P}_{w0} + 6s_{P_{w0}}$ and $T_{lo} = \bar{P}_{w0} + 3s_{P_{w0}}$ respectively. \bar{P}_{w0} is the mean wall pressure of the undisturbed turbulent boundary layer, and $s_{P_{w0}}$ is the standard deviation of the pressure signal.

Particle Image Velocimetry

The PIV image acquisition system used in the current study is shown in Fig. 8. The light source of the system was a double-pulse capable Spectra-Physics PIV-400 Nd:YAG laser. The energy per pulse was about 55 (± 10) mJ. A 1000x1000 pixel CCD camera (Kodak ES 1.0), capable of capturing sequential pulses separated by 1 μ s to 250 μ s on separate frames, was used. The pulse delay time, Δt , was 1 μ s. With this Δt the maximum particle displacement was less than 0.03 in. (0.76mm).

Three delay/pulse generators (Stanford Research Systems DG535) were used to drive the system. The first one generated a 10 Hz signal to drive the oscillators and Q-Switches in the PIV-400 laser. The second was triggered externally by the first one and provided the triggering signals for the acquisition of fluctuating pressure signals and the third DG535. The third one was used for triggering the CCD camera and setting up the timing electronics accurately for the laser pulses. The two pulses were monitored using a fast photodiode which was connected to a digital oscilloscope (Tektronix TDS 520C).

The particles used were aluminum oxide (Al_2O_3) with a manufacturer's specification of 0.3 μ m diameter, and were delivered using a two-stage fluidized-bed seeder. During a tunnel run, when the stagnation pressure reached a steady value, a valve that connects a nitrogen source to the fluidized-bed was opened to drive the particles into the flow through a streamlined injector. The injector was installed on the floor just downstream of the nozzle, 28 in. (71 cm) upstream of the blunt fin. The injector is 0.6 in (1.52 cm) high by 0.55 in. (1.4 cm) wide by 4.3 in. (10.9 cm) long in the streamwise direction. The leading and trailing edge surfaces were swept towards the center of the injector, yielding an appearance akin to a tapered diamond shape. To assess the potential interference of the injector on the interaction region, fluctuating pressure measurements were made with and without the injector in place. Fig. 9 shows the normalized power spectra of the signals recorded by the third upstream transducer for two different cases: i) undisturbed flow, with no injector in place, and ii) disturbed flow with injector in place and particle injection. The sampling frequency was 50 kHz and the signals were filtered at 20 kHz. The figure shows that the power spectrum for the disturbed case agrees well with that of the undisturbed case. The fact that the intermittency values for the transducers for the undisturbed and disturbed cases are very close suggest that disturbing the flow with injector and particle seeding does not have a significant effect on the dynamics of the flow in the interaction region.

The field of view for the PIV images was a 1.15 in (2.92cm) square window and its center was located 5.7 in. (14.5cm) from the leading edge of the blunt fin (Fig. 10). In the processing of the image pairs, the 1000x1000 pixel images were processed using an interrogation window of 64x64 pixels and an overlap of about 50%. This approach produced a 32x32 vector field with a resolution of about 1mm x 1mm for each vector. The images were processed on a Linux workstation using a PIV program developed in-house.²⁴⁻²⁵

Validation of the vector fields was performed based not only on the signal-to-noise ratio, but also on a priori knowledge of the flowfield: in a high Reynolds boundary layer vectors are nearly horizontal. After the validation, the holes were filled using an interpolation scheme. More than 5000 image pairs were obtained (after excluding those with problems) in the current study. The mean velocity profile was obtained by using all the retained vector fields. The fluctuation vector fields were then obtained by subtracting the mean velocity profile from the instantaneous vector fields.

Results and Discussion

Ensemble-Average Profiles of Velocity Fluctuations

One particular difficulty of the simultaneous PIV and fast response pressure measurements is that during the acquisition of the image and pressure data the transducers were exposed to the aluminum oxide particles. The most downstream transducer, being under the recirculating region, was affected the most. To minimize the impact of this problem the transducers were cleaned after each run. Also to reduce the exposure time of the transducers to the particles, the data acquisition time was limited to 13 seconds. In addition, before using the acquired data in any type of analysis, all the pressure as well as the image data were visually inspected, and when problems found, the corresponding image pairs and pressure segments were discarded. Sample pressure signals recorded by the transducers in the intermittent region are plotted in Fig. 11. These signals are typical of the intermittent region: the signals from the upstream channels show characteristics of less intermittent signals whereas the signals from downstream channels are of high intermittency.

In their work, Beresh *et al.*¹⁸ found a significant correlation between the velocity fluctuations in the lower part of the incoming boundary layer and the shock foot motion in the intermittent region. The same analysis approach was adopted for the blunt fin-induced interaction. Using a conditional analysis algorithm the image pairs were categorized for five different shock foot motions: upstream and downstream motions of one and two transducer spacings, and no motion at all. Similar to Beresh *et al.*,¹⁸ only the unidirectional shock motions were taken into account. This approach decreased the number of images for analysis but reduced potential effects from more than one type of boundary layer velocity fluctuation.

Conditional mean profiles of the velocity fluctuations were acquired for three different triggering time periods of 100 μ s (10 kHz), 250 μ s (4 kHz), and 500 μ s (2 kHz). The resulting mean profiles of the velocity fluctuations for a time window corresponding to 10 kHz are shown in Fig. 12. The figure shows the current results of the blunt fin case (Fig. 12a) as well as those of the compression ramp study (Fig. 12b)¹⁸ for comparison. The numbers in parentheses in Fig. 12a correspond to the number of image pairs included in ensemble averaging. It can be seen that in the lower part of the boundary layer there is a significant correlation between the velocity fluctuations and the specific shock motions. The positive velocity fluctuations correlate with the downstream motions of the separation shock foot whereas the negative velocity fluctuations correlate with the upstream motion of the

shock foot. This result is consistent with that of the compression ramp case as well as with the large eddy simulations of Hunt and Nixon,²⁶ which showed an approximately one-to-one relationship between the shock velocity and the incoming turbulent velocity fluctuations.

The mean profiles of the velocity fluctuations for a time window corresponding to 4 kHz are shown in Fig. 13. The corresponding compression ramp velocity fluctuations were given before (Fig. 5). When compared to the 10 kHz window, the trend for the 4kHz window for the blunt fin is similar, although there are some differences such as the "shock stationary" case near the wall. One reason for this particular case might be the considerably smaller number of samples (40% of those in the 10 kHz window): within a longer time period the shock has a higher probability to move a given distance, as compared to a shorter time period, hence a smaller number of images is unavoidable.

The fluctuation profiles for the 2 kHz window were also obtained (not shown). However, no significant correlations were found in this case. This is in agreement with the compression ramp case where the correlations for 2 kHz window were also significantly reduced.¹⁸

Discussion and Conclusions

The correlation seen in the blunt fin case is qualitatively similar to that obtained in compression ramp flows – negative velocity fluctuations in the lower part of the incoming boundary layer correlate with upstream shock motions and vice versa for motions of the separation shock that occur at frequencies less than 4 and 10 kHz. Since the large-scale structures in the outer part of the boundary layer have a characteristic frequency of order $U_\infty/d_0 = 40$ kHz, the source of the velocity fluctuations is likely not these outer-scale structures. This latter point is confirmed by the PLS visualization studies of Beresh *et al.*¹⁷ It is not known if these lower frequency fluctuations are a natural feature of the boundary layer turbulence, or are perhaps due to more coherent perturbations such as those generated by Görtler vortices or acoustic resonances in the plenum.

Although the source of the fluctuations is not known, Figs. 5 and 12 show that the magnitude of the velocity fluctuations, which correlate with the shock motion, is at least of order 20-30 m/s (note that it is entirely possible that the fluctuations could continue to increase closer to wall). Interestingly, the magnitude of these fluctuations is about 2-4% of the freestream velocity, which is about the same as the mean shock velocity measured in a range of different interactions including swept and unswept compression ramps and blunt fins.²⁷ As noted earlier, these results are also consistent with the large-eddy

simulations of Hunt & Nixon,²⁶ who found the separation shock foot velocity fluctuations closely followed the velocity fluctuations in the upstream boundary layer.

The present results are also consistent with previous results that show the separation shock-velocity and the wall-pressure-ratio across the shock are weakly correlated, with a negative time delay at peak correlation.⁶ Importantly, the negative time delay implies that the pressure ratio fluctuations *precede* the shock velocity fluctuations, thus suggesting a cause-and-effect relationship.

Finally, it is also interesting to consider the present results in the light of the work of Gonzalez and Dolling²⁷, who showed that the mean and root-mean-square of the shock speeds are essentially constant irrespective of model geometry and intermittent region length. They also showed that the separation shock Strouhal number defined using intermittent region length, maximum shock zero crossing frequency, and freestream velocity is essentially constant. The fact that some of the separation shock characteristics appear to be insensitive to the downstream flowfield/model geometry lends implicit support to the idea that the upstream effects play a more significant role in the separation shock unsteadiness than the downstream effects.

Although it cannot be stated with certainty that the dominant mechanism of shock motion has been identified in the case of compression ramp and blunt fin interactions, it is clear that these two flows, whose overall flow structures are quite different and whose length scales depend on different parameters, do share at least one common mechanism. Future work will be directed at testing several important implications of this mechanism.

Acknowledgment

Support for this research has been provided through Grants DAAG55-98-1-0062 and DAAG55-98-1-0290 from the Army Research Office monitored by Dr. T. Doligalski. The authors gratefully acknowledge this support.

References

- ¹Knight, D.D., and Degrez, G., "Shock Wave Boundary Layer Interactions in High Mach Number Flows. A Critical Survey of Current Numerical Prediction Capabilities," AGARD Advisory Report 319, Vol. II, pp. 1.1-1.35, Dec. 1998.
- ²Dolling, D.S., "Fluctuating Loads in Shock Wave / Turbulent Boundary Layer: Tutorial and Update," AIAA Paper 93-0284, Jan. 1993.

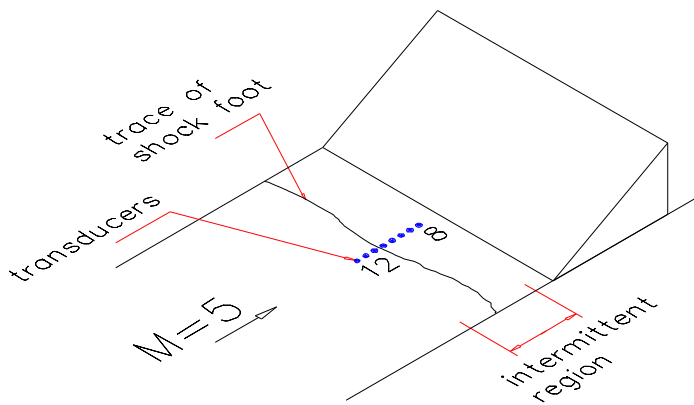
- ³Gramann, R.A., and Dolling, D.S., "Dynamics of Separation and Reattachment in a Mach 5 Unswept Compression Ramp Flow," AIAA Paper 90-0380, Jan. 1990.
- ⁴Erengil, M.E., and Dolling, D.S., "Correlation of Separation Shock Motion with Pressure Fluctuations in the Incoming Boundary Layer," *AIAA Journal*, Vol. 29, No. 11, 1991, pp. 1868-1877.
- ⁵Erengil, M.E., and Dolling, D.S., "Unsteady Wave Structure near Separation in a Mach 5 Compression Ramp Interaction," *AIAA Journal*, Vol. 29, No. 5, 1991, pp. 728-735.
- ⁶Erengil, M.E., and Dolling, D.S., "Physical Causes of Separation Shock Unsteadiness in Shock Wave/Turbulent Boundary-Layer Interactions," AIAA Paper 93-3134, July 1993.
- ⁷McClure, W.B., "An Experimental Study of the Driving Mechanism and Control of the Unsteady Shock Induced Turbulent Separation in a Mach 5 compression Corner Flow," Ph.D. Dissertation, Dept. of Aerospace Engineering and Engineering Mechanics, The University of Texas at Austin, Austin, TX, Aug. 1992.
- ⁸Dolling, D.S., and Brusniak, L., "Separation Shock Motion in Fin, Cylinder, and Compression Ramp Induced Turbulent Interactions," *AIAA Journal*, Vol. 27, No. 6, 1989, pp. 734-742.
- ⁹Ünalms, Ö.H., and Dolling, D.S., "Decay of Wall Pressure Field and Structure of a Mach 5 Adiabatic Turbulent Boundary Layer," AIAA Paper 94-2363, June 1994.
- ¹⁰Chan, S.C., Clemens, N.T., and Dolling, D.S., "Flowfield Imaging of Unsteady, Separated Compression Ramp Interactions," AIAA Paper 95-2195, June 1995.
- ¹¹Beresh, S.J., Clemens, N.T., Dolling, D.S., and Comninou, M.C., "Investigation of the Causes of Large Scale Unsteadiness of Shock-Induced Separated Flow Using Planar Laser Imaging," AIAA Paper 97-0064, Jan. 1997.
- ¹²Marshall, T.A., and Dolling, D.S., "Spanwise Properties of the Unsteady Separation Shock in a Mach 5 Unswept Compression Ramp Interaction," *AIAA Journal*, Vol. 30, No. 8, 1992, pp. 2056-2065.
- ¹³Spina, E.F., "Organized Structures in a Supersonic Turbulent Boundary Layer," Ph.D. Dissertation, Dept. of Mechanical and Aerospace Engineering, Princeton University, Princeton, NJ, Oct. 1988.
- ¹⁴Ünalms, Ö.H., "Structure of the Supersonic Turbulent Boundary Layer and Its Influence on Unsteady Separation," Ph.D. Dissertation, Dept. of Aerospace Engineering and Engineering Mechanics, The

University of Texas at Austin, Austin, TX, Aug. 1995.

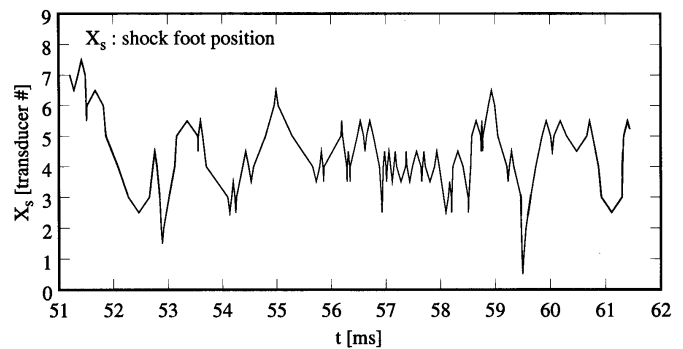
- ¹⁵Ünalmsis, Ö.H., and Dolling, D.S., "On the Possible Relationship between Low Frequency Unsteadiness of Shock-Induced Separated Flow and Görtler Vortices," AIAA Paper 96-2002, June 1996.
- ¹⁶Ünalmsis, Ö.H., and Dolling, D.S., "Experimental Study of Causes of Unsteadiness of Shock-Induced Turbulent Separation," *AIAA Journal*, Vol. 36, No. 3, March 1998, pp. 371-378.
- ¹⁷Beresh, S.J., Comminos, M., Clemens, N.T., and Dolling, D.S., "The Effects of the Incoming Turbulent Boundary Layer Structure on a Shock-Induced Separated Flow," AIAA Paper 98-0620, Jan. 1998.
- ¹⁸Beresh, S.J., Clemens, N.T., and Dolling, D.S., "The Relationship between Upstream Turbulent Boundary Layer Velocity Fluctuations and Separation Shock Unsteadiness," AIAA Paper 99-0295, Jan. 1999.
- ¹⁹Wu, P., and Miles, R.B., "MHz Rate Visualization of Separation Shock Wave Structure," AIAA Paper 2000-0647, Jan. 2000.
- ²⁰Kaufman, L.G., II, Korkegi, R.H., and Morton, L.C., "Shock Impingement Caused by Boundary Layer Separation Ahead of Blunt Fins," *AIAA Journal*, Vol. 11, No. 10, 1973, pp. 1363-1364.
- ²¹Saida, N., and Hattori, H., "Shock Wave-Turbulent Boundary Layer Interactions Induced by a Blunt Fin,"

Trans. Japan Soc. Aero. Space Sci., Vol. 27, No. 76, 1984, pp. 67-77.

- ²²Fomison, N.R., and Stollery, J.L., "The Effects of Bluntness on a Glancing Shock Wave Turbulent Boundary Layer Interaction," AGARD CP 428, 1987.
- ²³Kleifges, K., and Dolling, D.S., "Leading-Edge Sweepback and Shape Effects on Fin-Induced Fluctuating Pressures," *Journal of Spacecraft and Rockets*, Vol. 32, No. 2, 1995, pp. 286-293.
- ²⁴Beresh, S.J., "The Effects of the Incoming Turbulent Boundary Layer on a Shock-Induced Separated Flow using Particle Image Velocimetry," Ph.D. Dissertation, Dept. of Aerospace Engineering and Engineering Mechanics, The University of Texas at Austin, May 1999.
- ²⁵Rehm, J.E., "The Effects of Heat Release on Planar Jet Diffusion Flames," Ph.D. Dissertation, Dept. of Aerospace Engineering and Engineering Mechanics, The University of Texas at Austin, Dec. 1998.
- ²⁶Hunt, D., and Nixon, D., "A Very Large-Eddy Simulation of an Unsteady Shock Wave/Turbulent Boundary Layer Interaction," AIAA Paper 95-2212, 1995.
- ²⁷Gonzalez, J.C., and Dolling, D.S., "Correlation of Interaction Sweepback Effects on the Dynamics of Shock-Induced Turbulent Separation," AIAA Paper 93-0776, Jan. 1993.



(a)



(b)

Fig. 1 Sample shock foot history in a Mach 5 compression ramp interaction:
a) schematic of experiment b) shock foot history (Ref. 2).

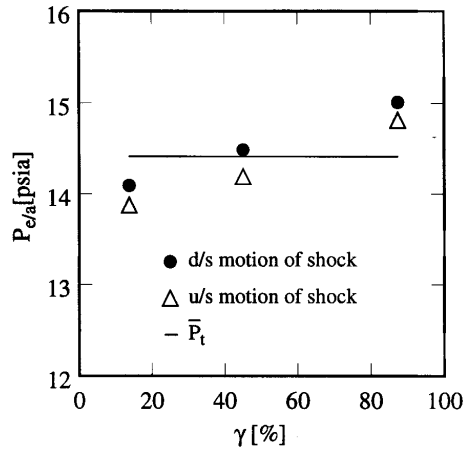


Fig. 2 Ensemble-averaged Pitot pressure as a function of intermittency (Ref. 9).

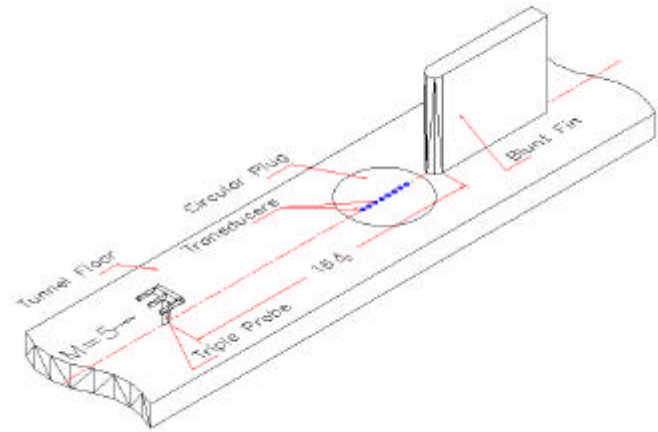


Fig. 3 Triple-tipped Pitot probe upstream of a blunt fin (Ref. 16).

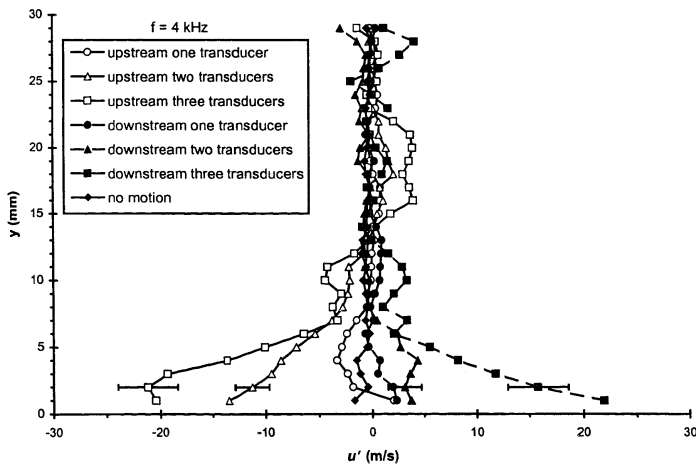


Fig. 5 Conditional ensemble average profiles of the streamwise velocity fluctuations in the incoming boundary layer conditioned upon the separation shock foot motion within a time period corresponding to 4 kHz in a compression ramp-induced separated flow (Ref. 18).

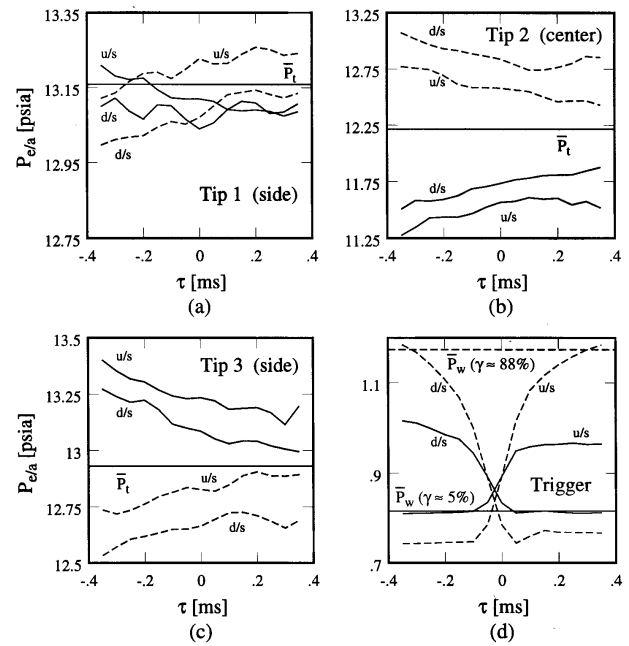


Fig. 4 Ensemble-averaged pressure histories for certain positions and motions of shock foot
 —: large separated flow (shock foot is upstream)
 ---: small separated flow (shock foot is downstream)
 u/s: upstream motion of shock foot
 d/s: downstream motion of shock foot
 (a) triple probe - Tip 1 (b) triple probe - Tip 2
 (c) triple probe - Tip 3 (d) triggering channel (Ref. 16).

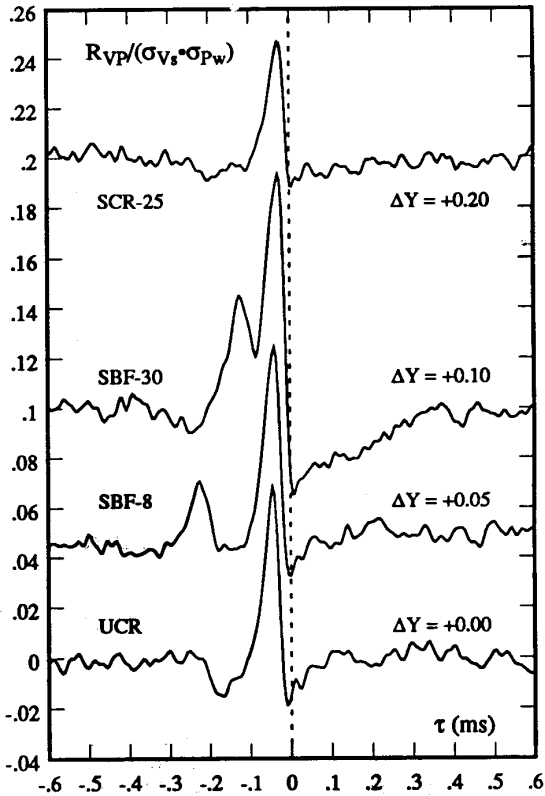


Fig. 6 Normalized cross-correlation of shock velocity and upstream pressure.
 SCR-25: 25 deg swept compression ramp
 SBF-30: 30 deg swept blunt fin
 UCR: unswept compression ramp
 ? Y: offset
 s_{Vs} : standard deviation of shock velocity
 s_{Pw} : standard deviation of wall pressure
 R_{Vp} : cross correlation of shock velocity and wall pressure (Ref. 6).

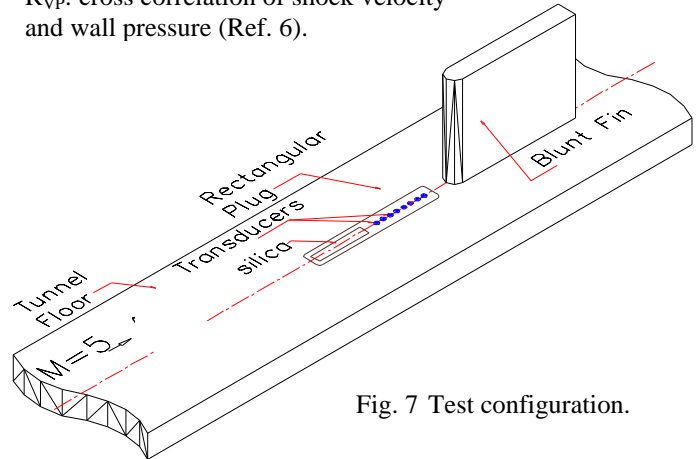


Fig. 7 Test configuration.

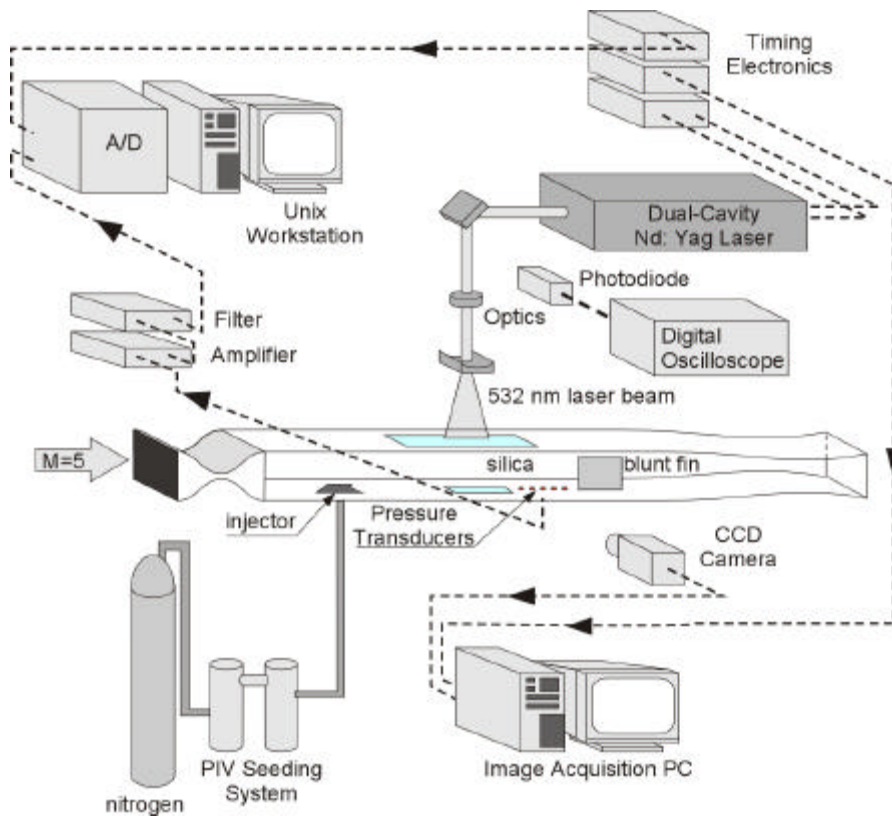


Fig. 8 Experimental set-up for particle image velocimetry (PIV) experiments.

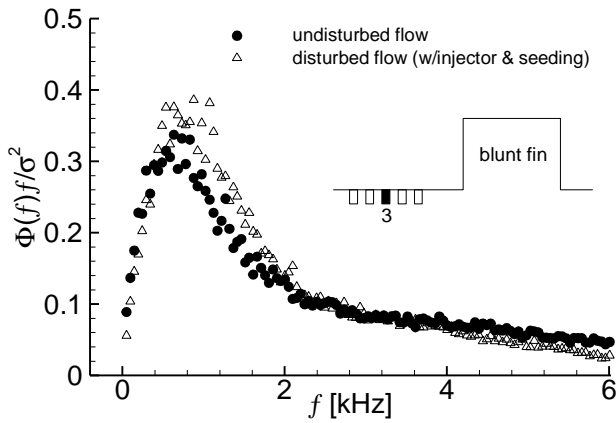


Fig. 9 Effect of injector and seeding on the pressure power spectra of transducer 3.

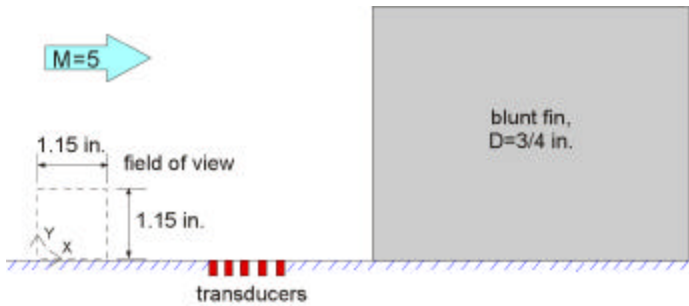


Fig. 10 The field-of-view for the PIV window, transducers and the blunt fin.

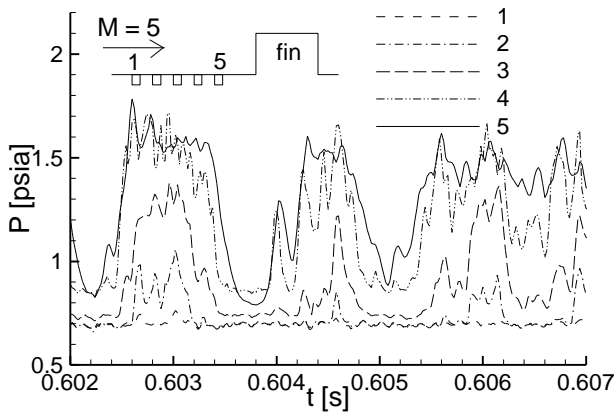


Fig. 11 Sample pressure histories of the transducers in the intermittent region.

Fig. 13 Conditional ensemble average profiles of the streamwise velocity fluctuations in the incoming boundary layer conditioned upon the separation shock foot motion within a time period corresponding to 4 kHz in a blunt fin-induced separated flow.

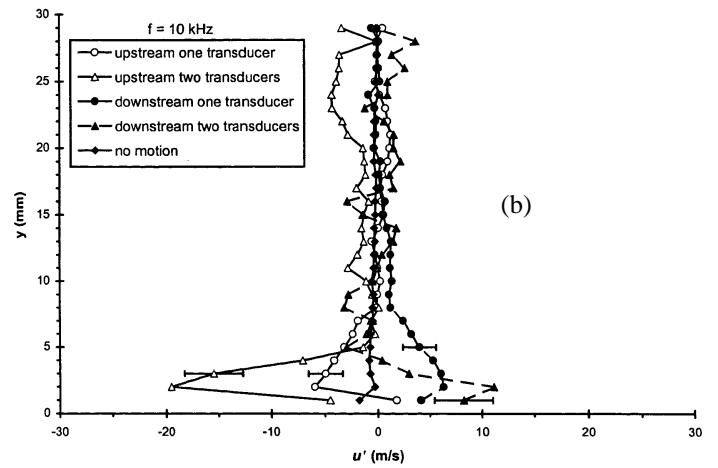
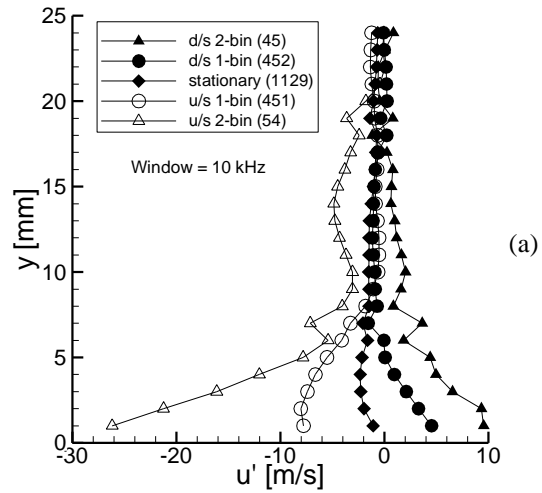


Fig. 12 Conditional ensemble average profiles of the streamwise velocity fluctuations in the incoming boundary layer conditioned upon the separation shock foot motion within a time period corresponding to 10 kHz:
a) blunt fin case (current work)
b) compression ramp case (Ref. 18).

